Correction factors for monitor unit verification of clinical electron beams

Abstract:

Purpose: We provide heterogeneity and geometry correction factors for use in electron monitor unit verification calculations. **Method:** We use the unrestricted collisional stopping power for tissues encountered in electron beam treatments to make the heterogeneity correction factors table. We create the geometric correction factors table by taking the ratio of the doses in spherical phantoms to the dose in a flat phantom. We then added the correction factors to the TG-71 monitor unit verification equation. **Results:** The heterogeneity and geometry correction factors range from (0.9-1.01) and (0.8-1.0), respectively, for the energies presented. The differences between the treatment planning system and the TG-71 calculations drop from (3-14)% to (0-3)% using our modified equation. **Conclusion:** Monitor units calculated with the correction factors typically increase for patients with a convex curvature, which matches the behavior of Monte Carlo based planning algorithms. An increase in monitor units lowers the percent difference between the second check and the treatment planning system to under the TG-114 recommended 5% actionable level.

Introduction

The current guidance for calculating dose distributions and monitor units (MU) for clinical electron beams is to use CT datasets and 3D heterogeneity corrections [1]. The recommendation assumes the treatment planning system (TPS) is properly commissioned following the guidelines in TG-53 [2]. However, anecdotal evidence suggests that there are a large number of centers that utilize their TPS for the calculation of electron isodose lines, yet choose to treat the planned aperture and geometry with hand or second check calculated MU rather than the MU from the TPS[3].

At our institutions, when modeling dose in the breast, chest wall, and scalp, the MU calculated by the treatment planning system (Eclipse eMC, Varian Medical Systems, Palo Alto, CA) are generally greater than the MU calculated using the TG-71[4] formalism. TG-114 and TG-71 indicate that patient heterogeneity and complex geometries (obliquity and patient curvature) are the most likely causes [5, 4]. Khan has discussed obliquity factors for electron beams[6], and those treatment types are not considered here. Our focus in this study is *en face* treatment beams. We denote the corrections associated with patient curvature as geometry corrections. Below we present tables of heterogeneity and geometry correction factors. These factors are sufficient to correct hand calculations in several anatomic locations using *en face* treatment beams.

Method

Unless stated otherwise, all TPS calculations include heterogeneity corrections and an appropriate grid resolution, smoothing level, and particle history count[7, 8]. The reference point depth used for normalization is d_{max}. The d_{max} reference point is the depth of maximum dose as measured using a 10×10 electron cone in calibration conditions for the energy under consideration[9]. All calculations use this

depth regardless of cutout size, patient curvature, or heterogeneity for dose normalization and factor calculation.

A. Geometry correction factors using the TPS

We calculated the geometry factors (GF) using the following procedure. We began with a flat water phantom and a set of water equivalent spheres with radii of 3, 5, 7, 10, and 15 cm drawn in the treatment planning system. On the flat water phantom, we added the reference point at the depth corresponding to the calibration beam d_{max} for the selected energy. The beam SSD was constant at 100 cm. Next, we calculated the dose to the reference point with 100 MU, giving the baseline dose for this cone and energy combination.

We repeated the above steps with each of the spheres, making sure to align the center of the beam to the same reference point as the flat phantom. We calculated all configurations three times using different random seeds for all energies and cones typically used in our clinics: 6, 9, and 12 MeV. When the standard deviation of the calculated reference point doses was greater than the uncertainty of the Eclipse calculation, we substituted the mean dose to a spherical volume with a radius of 0.8 cm surrounding the reference point.

To estimate the uncertainty in each value of GF per institution, we calculated the standard deviation of the dose over the three calculations. We followed the formalism of Lichten[10] to calculate the error in GF, assuming the equation for GF is a/b, where a is the reference point dose in the sphere, and b is the reference point dose in the flat phantom. We used the resulting average GF from each of our centers for each energy and sphere combination to calculate a final weighted average GF. We calculated a

maximum uncertainty in the final GF by combining the error from each institutions' GF in quadrature. Below we will focus on the GF calculated using the 10x10 cone because there was no difference in GF for different cone sizes within the uncertainty of the calculations.

We fit the 10×10 final GF for each energy using Equation 1.

Equation 1

$$GF = a\ ln(r)^2 + b\ ln(r) + c,$$

where r is the radius of the sphere. We use the functional form to find the geometry factor at any radius.

B. Phantom Measurements as Verification

To verify our calculated correction factors from the TPS, we measured the dose in phantoms which mimic a spherical geometry using a Sun Nuclear IVD2 with the electron QEDs (Sun Nuclear Corporation, Melbourne, FL). To calibrate the IVD2 and QEDs, we used a reference setup (10x10 cone at 100 cm SSD) for each energy and delivered 200 MU, giving 200 cGy to the reference point. We measured the dose at the same depth as the reference setup with the following phantoms. First, we used a Lucy 3D phantom (Standard Imaging, Middleton, WI). We taped the electron QED to the surface of the Lucy. We placed the correct depth of sticky bolus on the QED so that the QED was as close as possible to the reference point for the energy measured. We used kV images of each setup to verify the accuracy of the positioning for the QED and the TSD. We imported the images into the EMR and drew circles that matched the curvature for each setup. Figure 1 shows the kV image and configuration for the Lucy 3D phantom. We used other items in the clinic to create more spherical phantoms including: a styrofoam hemisphere used for setting up OSMS, a High Bounce Pinky rubber ball, and a mannequin used for OSMS

QA. For the styrofoam dome, we placed 1 cm of bolus on the surface of the styrofoam hemisphere, under the QED, to maintain backscatter. For the high bounce rubber ball, we cut the ball to depths of 2 cm and 3 cm, corresponding to the 9E and 12E energies reference points for a very small, 3 cm, radius of curvature. The mannequin is a thin shell meant for displaying clothes. We placed bolus on the inner portion of the shell and held it in place with a second mannequin shell underneath (Figure 2). We kept the bolus above the QED and the TSD the same for all phantoms. All measurements had an en face beam defined by a 10x10 cone with a 10x10 cm^2 standard cutout, 200 MU, 1000 MU/min dose rate, and 100 cm SSD to the bolus surface.

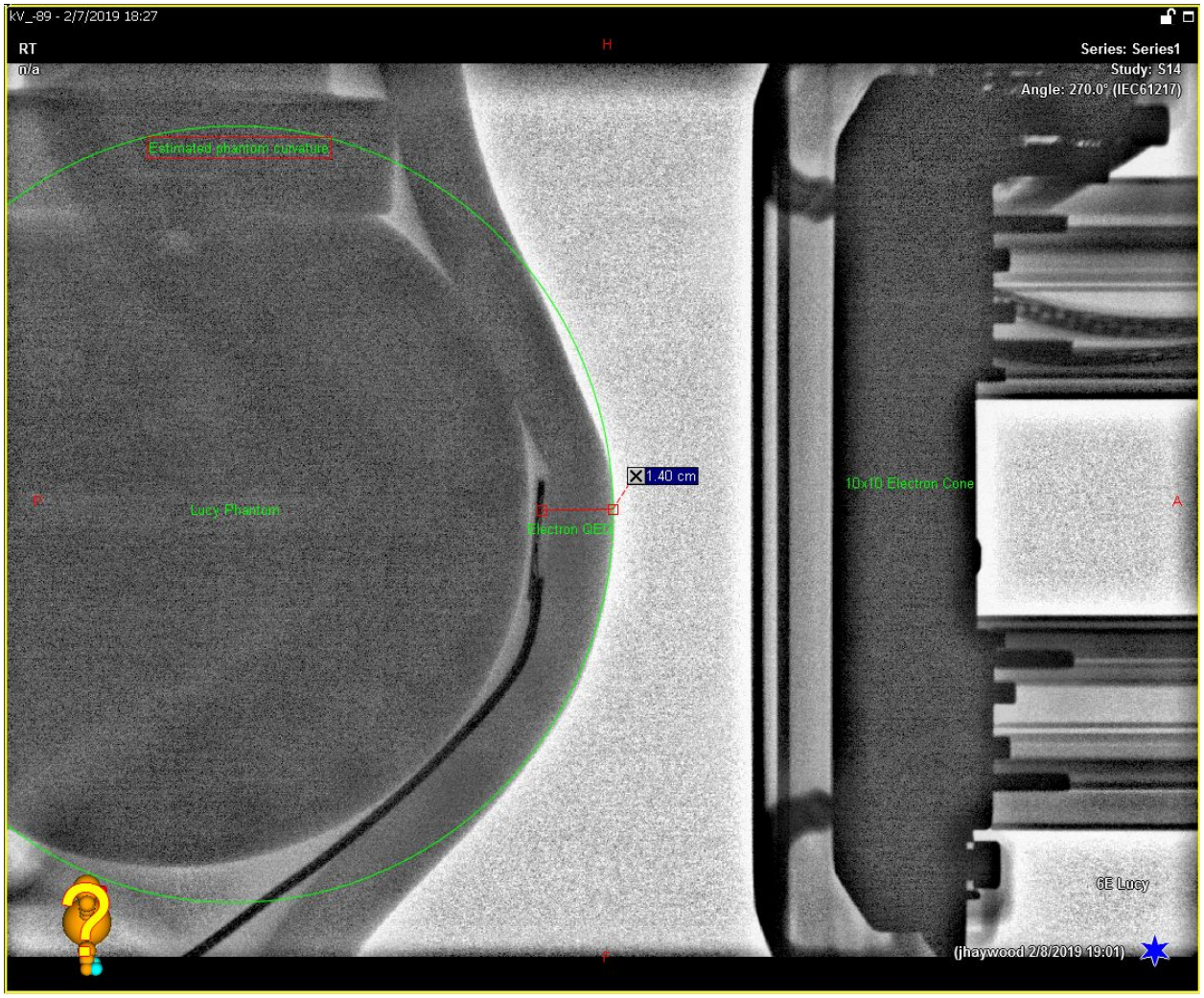

Figure 1: kV image of the Lucy 3D phantom with the electron EQD taped to the surface. 1.5 cm of sticky bolus covers the QED. The radius of the green circle determines the radius of the spherical phantom setup and thus GF.

Figure 2: Mannequin setup for the 12E beam. There is 3 cm bolus over the QED. We centered the bolus and QED on the breast of the phantom. The second mannequin is underneath to hold the inner bolus in place. For this setup, the gantry angle was 10 degrees to make this an enface beam.

C. Calculating MU

To calculate the second check MU, we used equation 12 of TG-71 [4]. Eclipse reports a dose to medium and a hand calculation assumes a dose to water. We rearrange Equation 8.69 from[6] to calculate the dose to water based on the dose to medium,

Equation 2

$$D_{water} = D_{medium} \times \left(\frac{\bar{S}}{\rho} \right)_{medium}^{water} = D_{medium} \times \left(\frac{S_c^{water}}{S_c^{medium}} \right) = D_{medium} \times \frac{1}{HET}.$$

S_c is the unrestricted collision stopping power from the NIST ESTAR database[11]. HET is the ratio of S_c at the energy of the electron beam at the reference point for the medium and water. The energy at depth z in water is, using equation 14.7 from[6],

Equation 3

$$\overline{E}_z = \overline{E}_0\left(1-\frac{z}{R_p}\right).$$

With the heterogeneity and geometry correction factors, we modify Equation 12 of TG-71 [4] to,

Equation 4

$$MU = \frac{Dose_{medium}\times 100}{D_0^{'}\times PDD(d,r_a,SSD_0)\times S_e(r_a,SSD_0)\times InvSqr\times HET\times GF}$$

We have added HET, the heterogeneity correction factor, and GF, the geometry correction factor. We use a percent difference to compare the corrected MU calculated using Equation 4 to the Eclipse and TG-71 MU.

C. 1. Estimating the patient heterogeneity at the calculation point

For patient heterogeneity factors, we use the physical material composition supplied by Eclipse. The NIST Material Composition database [11] lists the density of various tissues commonly found in radiation therapy. We chose the medium that most closely matches the Eclipse density. Most likely, one or a combination of the following will match; adipose, muscle, bone, water, or skin. In the NIST ESTAR database, we found the unrestricted collisional stopping power, S_c, for the energy of the beam at the reference point for the selected medium and water. When more than one material was present, we used a weighted average to determine S_c. We used Equation 3 to calculate the energy at depth regardless of the medium.

HET represents the correction if only that material is present in the patient. When the beam passes various materials, we use a weighted average to determine HET. For example, a 6 MeV treatment for a scalp with 1 cm bolus with the reference point located 3 mm deep in bone and total depth of 1.3 cm will have HET given by,

Equation 5

$$HET = \frac{d_{Bone} \times HET_{Bone} + d_{Water} \times HET_{Water}}{d_{Max}} = \frac{0.3 \times 0.905 + 1.0 \times 1.000}{1.3} = 0.978.$$

C. 2. Estimating the curvature of the Patient

We found the curvature of the patient using the drawing and contouring tools in Eclipse. First, we center all views on the reference point and rotate the views so that two planes are orthogonal to the beam's eye view. We draw a circular contour that matches the patient's anatomy on the orthogonal views. As an example, Figure 3 shows the outline used to estimate the transverse curvature in the ART phantom for an orbit calculation. The patient radius of curvature used in Equation 1 is the average of the radii of these two contours.

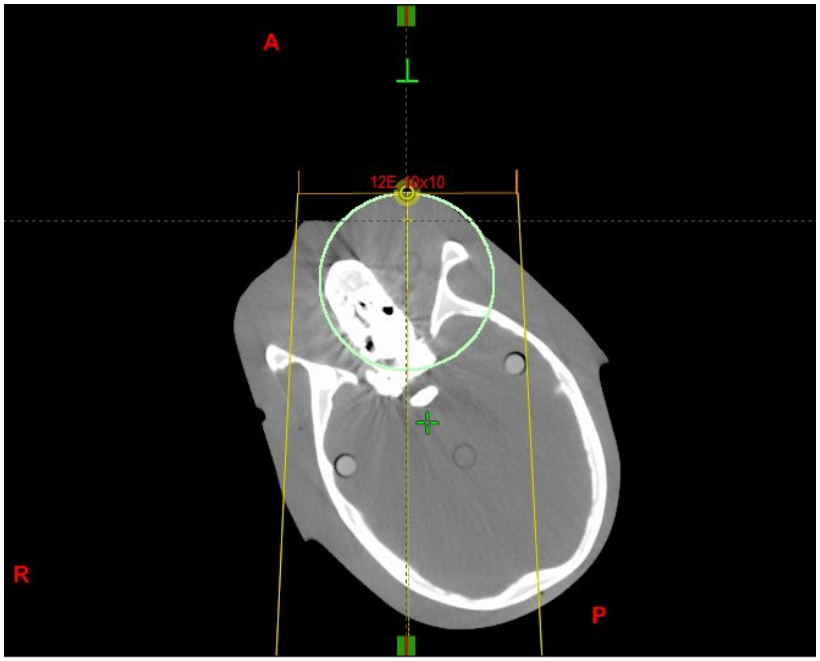

Figure 3: Example contour used to estimate the transverse radius of curvature.

Results

A. Phantom correction Factors using the TPS

The geometry correction for a given sphere is the dose at the reference point in the sphere divided by the dose to the reference point on the flat phantom. In Table 1, we provide the 10×10 cone final GF for the 6, 9, and 12 MeV energies computed from all data from both institutions. We limit Table 1 to only the 10x10 cone because factors calculated for the other cones and energy combinations were the same as the 10x10 cone within the calculation uncertainty. Finally, Table 2 shows the coefficients of Equation 1 fitted to the GF data in Table 1 for each energy. The uncertainty in the fitted coefficients is reported directly from the fitting software.

Table 1: 10x10 final GF. GF for other energy and cone combinations are the same within the calculated uncertainty.

10x10 Final GF						
Sphere Radius (cm)	**6 MeV**	σ	**9 MeV**	σ	**12 MeV**	σ
Flat	1.000	0.009	1.000	0.008	1.000	0.009
3	0.888	0.008	0.855	0.008	0.847	0.008
5	0.939	0.007	0.913	0.008	0.899	0.009
7	0.954	0.009	0.934	0.007	0.924	0.008
10	0.974	0.006	0.961	0.009	0.950	0.010
15	1.000	0.009	0.991	0.008	0.985	0.007

Table 2: a, b, and c fitted to Equation 1 for the 10x10 final GF of each energy in Table 1.

Energy (MeV)	**a**	σ_a	**b**	σ_b	**c**	σ_c
6	-0.0148	0.011	0.123	0.044	0.774	0.041
9	-0.0147	0.009	0.138	0.041	0.722	0.039
12	-0.0089	0.012	0.118	0.048	0.729	0.043

B. Measurement Results

Table 3 shows the measured doses and measured GF for all of the energy and phantom combinations. We also show the percent difference from the expected GF calculated using Equation 1. We did not collect data for the specific energy and phantom combinations that have empty cells due to clinical or physical limitations. For example, the rubber ball could not be cut to put the QED at the reference point for the 6E beam.

Table 3: Measured doses and GF for all of the phantom and energy combinations used along with the estimated radius of curvature and calculated GF.

Phantom					
Flat	**Energy (MeV)**	**6**	**6**	**9**	**12**
	Mean Dose (cGy)	200	199.7	199.6	199.6
Lucy	**Mean Dose (cGy)**	190.7	192.8	187.4	193
	Measured GF	0.954	0.965	0.939	0.967
	Measured Radius (cm)	7.5	7.5	8.5	11
	Calculated GF	0.961	0.961	0.952	0.962
	% difference	0.73%	0.42%	1.37%	0.52%
Dome	**Mean Dose (cGy)**	196.1	198.7	194.4	197
	Measured GF	0.98	0.995	0.974	0.987
	Measured Radius (cm)	15	15	16	18.5
	Calculated GF	0.997	0.997	0.994	0.998
	% difference	1.72%	0.20%	2.03%	1.11%
Rubber Ball (uncut with bolus)	**Mean Dose (cGy)**	-	191.6	185.9	190.2
	Measured GF	-	0.96	0.931	0.953
	Measured Radius (cm)	-	5.5	6.5	9
	Calculated GF	-	0.94	0.931	0.946
	% difference	-	2.11%	0.00%	0.74%
Rubber Ball (cut no bolus)	**Mean Dose (cGy)**	-	-	169.2	171
	Measured GF	-	-	0.847	0.857
	Measured Radius (cm)	-	-	3	3
	Calculated GF	-	-	0.857	0.849
	% difference	-	-	1.17%	0.94%
Breast	**Mean Dose (cGy)**	186.5	-	185.6	190.7
	Measured GF	0.933	-	0.93	0.954
	Measured Radius (cm)	6	-	7	8
	Calculated GF	0.946	-	0.937	0.937
	% difference	1.38%	-	0.75%	1.80%

C. Calculating MU

For demonstration, we present the TPS calculations necessary to decompose HET and GF from a typical patient treatment, a chest wall with a 10 cm radius curvature (Table 4). The heterogeneity correction factor is the average dose in the patient with heterogeneity corrections on divided by the average dose with the external contour density changed to water. The geometry correction is the average homogeneous dose calculated in the patient divided by the average dose calculated in the flat water phantom. We calculated the cutout factor by dividing the average dose with the cutout in the flat phantom by the average dose with the standard cutout in place.

Table 4: Calculation of heterogeneity, cutout, and geometry factors based on the TPS dose to the reference point.

Line	Calculation Step	Dose (cGy)	Calculation
a	Heterogeneous patient dose	185.2	
b	Homogeneous patient dose	188.0	
c	Cutout on flat water phantom dose	198.0	
d	10x10 water phantom dose	197.5	
e	Heterogeneity factor	0.985	a/b
f	phantom cutout factor	1.002	c/d
g	total correction factor	0.938	a/d
h	geometry factor	0.949	b/c

The MU calculated using the TG-71 equation for this chest wall scar boost are,

Equation 6

$$MU = \frac{Dose \times 100}{D_0' \times PDD \times S_e \times InvSqr} = \frac{200 \times 100}{1.0 \times 100 \times 1.012 \times 1.0} = 198.$$

Here, S_e is from the JFCC table of standard cutout factors. When we add in HET and GF from lines e and h of Table 4 the MU become,

Equation 7

$$MU_1 = \frac{200 \times 100}{1.0 \times 100 \times 1.012 \times 1.0 \times 0.985 \times 0.949} = 212.$$

We calculated the MU again by estimating HET from the unrestricted collision stopping power, S_c, for water and muscle, and the spherical geometry correction factors calculated in Table 4. The energy at the reference point in the 9 MeV beam is 4.4 MeV. We choose to use 4.5 MeV in the S_c tables. For muscle, S_c = 1.86 MeV cm^2/g, and for water, S_c = 1.882 MeV cm^2/g, and HET = 0.988. Then,

Equation 8

$$MU_2 = \frac{200 \times 100}{1.0 \times 100 \times 1.012 \times 1.0 \times 0.988 \times 0.961} = 208.$$

Table 5 lists the unrestricted collisional stopping powers and computed HET at the reference point for materials commonly encountered in the clinic: adipose, muscle, bone, skin, and water.

Table 5: Unrestricted collisional stopping powers and calculated HET for common materials.

Stated Energy	Energy at D_{Max} (Mev)	Sc				
		Adipose	**Muscle**	**Bone**	**Skin**	**Water**
6	3	1.872	1.824	1.670	1.822	1.846
9	4.5	1.909	1.860	1.709	1.858	1.882
12	6	1.939	1.889	1.740	1.888	1.911
		HET				
		Adipose	**Muscle**	**Bone**	**Skin**	**Water**
6	3	1.014	0.988	0.905	0.987	1.000
9	4.5	1.014	0.988	0.908	0.987	1.000
12	6	1.015	0.988	0.911	0.988	1.000

In Table 6 we show the MU calculated for various patient anatomies using the TG-71 formalism and using Equation 4 above. We use the HET factor from Table 5 after measuring the density of the medium in Eclipse. We measured the patient curvature in the two planes perpendicular to the beam's eye view. We calculated GF using Equation 1 with the coefficients for the corresponding energy from Table 2.

Table 6: MU calculations for various patient anatomies using the TG-71 equation and Equation 3 (Corrected MU) compared to the Eclipse MU.

Patient	1	2	3	4	5	6	7	8	9
Treatment Site	Breast	CW Scar	CW Scar	Scalp	Ear	CW Scar	CW Scar	Arm	Nose
Stated Energy	9	9	9	9	12	12	9	9	9
Cone Name	10x10	15x15	20x20	15x15	15x15	15x15	15x15	10x10	6x6
Cutout (cm)	7	10	15	12	11	15	10	9	4
Dose (cGy)	200	200	200	250	180	200	200	200	250
SSD (cm)	100	100	105	100	115	105	110	100	100
Gap (cm)	0	-1	4.5	-1	14	4	9	-0.5	0
PDD (%)	90	100	90	90	100	100	95	90	100
Depth (cm)	2.03	2.03	2.08	2.03	2.8	2.93	2.03	2.03	2.03
VSSD (cm)	89.5	89.5	89.5	89.5	89.9	90	89.5	89.5	89.5
Tissue	Muscle	Muscle	Adipose	Muscle	Bone	Muscle	Adipose	Adip Muscle	Muscle Cart.
Curvature (cm)	9 11	15 5	10 15	10 10	15 15	10 15	10 15	6 6	3 3
Se	1.006	1.003	0.993	1.001	1.002	0.994	1.003	1.01	0.933
Inverse Square	1.000	1.022	0.909	1.022	0.755	0.919	0.829	1.011	1.000
HET	0.988	0.988	1.014	0.988	0.911	0.988	1.014	1.009	0.986
Ave. GF	0.936	0.923	0.944	0.936	0.981	0.967	0.944	0.907	0.850
TG-71 MU	221	195	246	271	238	219	253	218	268
Eclipse MU	236	207	255	291	259	233	272	239	309
% Diff TG-71 MU vs Eclipse MU	7	6	3	7	8	6	7	9	14
Corrected MU	239	214	257	294	266	229	264	238	320
% Diff Corrected MU vs Eclipse MU	1	3	1	1	3	2	3	0	3

Discussion

A. Phantom correction Factors using the TPS

Each patient's geometry is independent but similar to all other patients. Thinking of the typical treatment sites in our clinic (breast, chest wall, scalp), all are convex. The convex geometry for an en face beam means the lateral portion of the isodose lines will be at deeper depths than on a flat phantom[6]. The lateral scatter that would generally add to the dose at a point on the central axis is now deeper in the tissue. One way to quantify the effect of the missing lateral scatter is to assume a spherical geometry. Spheres represent a simplification of the convex geometry presented by a patient. For example, a large sphere with 15 cm radius represents a chest wall, while a medium sphere with 8 cm radius represents a skull, and a small sphere with a 3 cm radius represents a nose with bolus.

Our first step was to confirm that a spherical geometry could be at least a first-order approximation to the patient geometry. Table 1 shows the geometry factor for a 9 MeV beam using a 10×10 cone with the 10×10 cm^2 standard insert. The patient calculations presented in Table 4 used this same beam configuration. We measured the radius of curvature for this patient to be 10 cm in both planes perpendicular to the beam's eye view. Within the statistical uncertainty of the calculations, ~1.5%, GF from Table 1 and Table 4 are the same. However, an agreement for one patient does not mean the spherical geometry is suitable for all patients. To test this, we calculated the geometry correction factor for a wide range of beam energies, field sizes, and sphere radii. We used these factors in the MU calculations (Equation 4) for a representative sample of patients from our clinics, see Table 6.

In Table 1, we only listed GF for the 10×10 cone. This is because, within the uncertainty of the calculations, we saw no difference in GF for different cone sizes when calculating with the same energy and sphere. For example, the 6 MeV GF for the 6×6 cone and 3 cm sphere was 0.889. This is included in the range of the 10×10 cone GF uncertainty, 0.888 ± 0.008. Another example, the 9 MeV GF for the 20×20 cone on a 7 cm sphere was 0.940, also within the expected range, 0.934 ± 0.007.

B. Measurement

The percent difference between the measured and calculated geometry factors presented in Table 3 ranges from 0 to ~2%. This is likely due to the uncertainty of the setup during the measurement. For example, the rubber ball was taped to the table, the QED was taped to the ball, then the bolus was placed over the ball and QED. We have used great care in the procedure, but the magnitude of the effect of the bolus shifting or tilting the QED, the ball remaining exactly centered, or the bolus stretching and thinning is unknown. We did take kV images of most measurements to verify the setup and do notice the angle of the QED is not perpendicular to the beam for every measurement. Figure 4 shows the rubber ball setup for one of the measurements. Also, the styrofoam dome, the rubber ball, and Lucy phantom will have different backscatter characteristics than water. We did not attempt to account for the heterogeneity of the setup, except for adding the 1 cm bolus on the styrofoam dome.

We have included the measured geometry factors for a few reasons. As mentioned above, some centers do not use the eMC MU. The GF may be a result of the eMC algorithm. Indeed, the eMC algorithm uses spheres to fit the patient's geometry (Eclipse algorithm reference guide, Varian Medical Systems, Palo Alto, CA). While it is unlikely the eMC algorithm is producing this GF artificially, the possibility is eliminated by the measurements. Next, the magnitude of the calculated geometry factors could be incorrect for several reasons: the lateral scattering is erroneous in the eMC algorithm, the assumption that spheres are the correct geometry could be wrong, we may have an unknown systematic error in our

calculations, etc. The overall percent difference between the measured and calculated GF is 1.0%. This shows the calculated GFs are due to the spherical geometry and not an unknown anomaly. The measurements ensure the calculated factors are correct and usable without reservation.

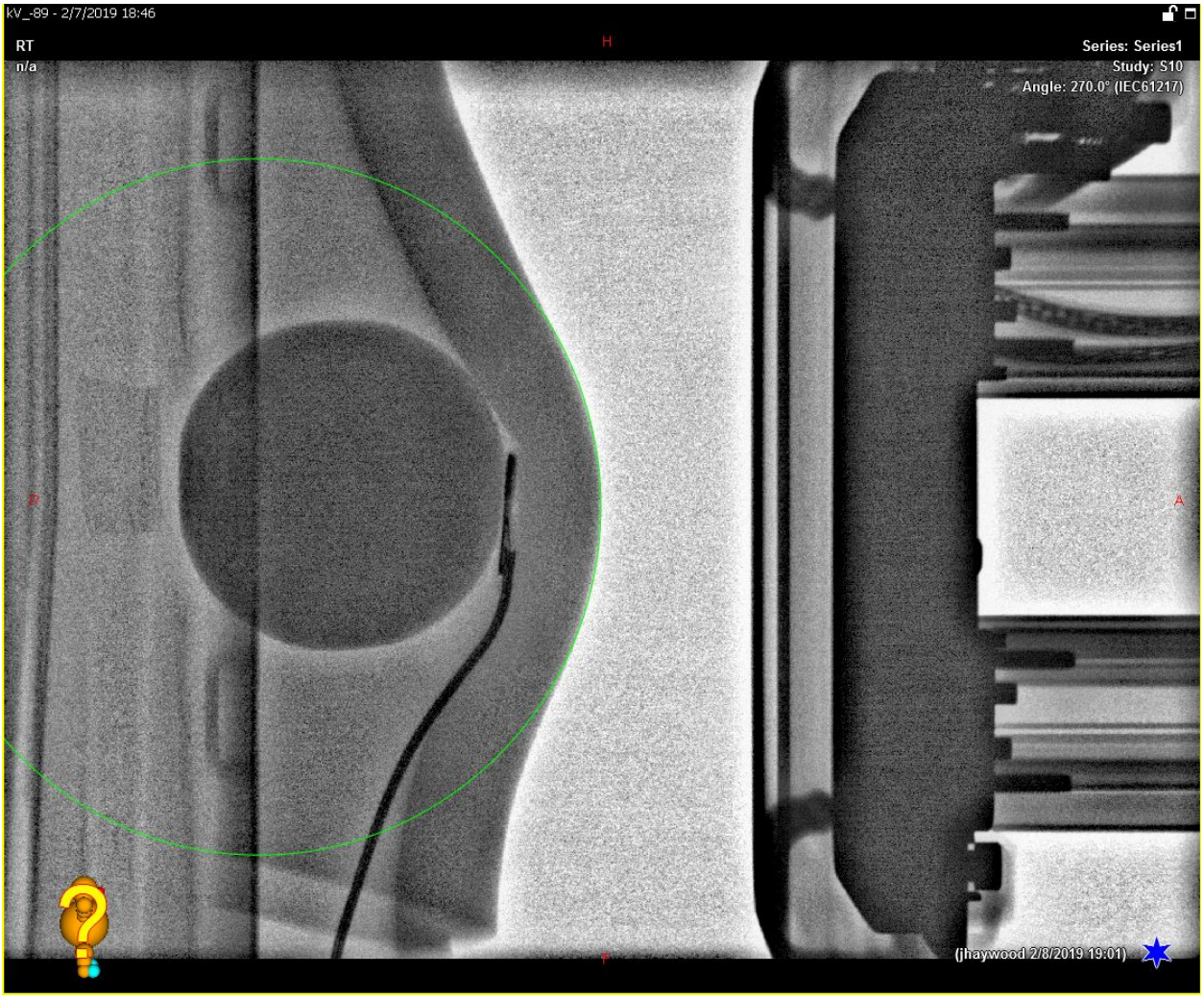

Figure 4: kV image of the rubber ball with 2 cm bolus and the electron QED in place. Note that the QED is angled with respect to the beam.

C. Calculating MU

The Eclipse dose decomposition to get the heterogeneity and geometry corrections for the patient has one major fault. It takes a long time to calculate each step. A lower energy beam, 9 MeV, with a small cone, 10×10, takes ~6 minutes to calculate with 160 million particle histories, ~1% accuracy. For a high energy beam, 12 MeV, in a large cone, 25×25, one calculation takes ~45 minutes for 1 % accuracy and 1 mm grid resolution. There are a total of 12 calculations presented in Table 4 and it would take between 1 - 9 hours to reproduce. A multiple hour second check calculation is unacceptable.

The calculation on the patient presented in Table 4 does show the magnitude of each correction. In agreement with TG-114, the heterogeneity and geometry factors introduce the greatest uncertainty [5]. A TG-71 MU calculation on this patient, which assumes HET and GF are 1.0, introduces a combined uncertainty in the resulting MU of, $\sigma_{MU} \approx \sqrt{(0.015)^2 + (0.051)^2} = 5\ \%$. While this falls within the action levels given in Table III of TG-114, we have not taken into account all of the uncertainty. Among other things, we have ignored the uncertainty of the cutout factor, 1 – 2 %, and the MU/dose calculated by Eclipse, 1 – 2 %. Including these uncertainties pushes σ_{MU} higher. Table 6 shows the percent difference between the TG-71 and Eclipse MU for a variety of patients. Only one of those patient calculations is within 5 %. By decomposing the MU calculation we see that for the majority of patients the geometry factor is the dominant contributor to large percent differences.

Equation 6 gives the TG-71 monitor units of 198 MU for the sample chest wall patient presented in Table 4. The MU calculated by Eclipse are 217 MU, a 9 % difference. With the correction factors added (Equation 7) MU_1 is 212 MU, a 2 % difference. The result shows that only the heterogeneity, cutout, and geometry factors are necessary to reproduce the Eclipse MU. MU_2 (Equation 8) uses the HET and GF factors that were calculated independently of the patient and gives 211 MU, a 3 % difference.

The patient calculations presented in Table 6 have percent differences between the TG-71 and Eclipse MU that range from 3 to 14 %. The percent differences between the corrected MU and Eclipse range from 0 to 3 %. All of the materials in Table 5 yield an HET that is constant over the energies presented, except for bone. Therefore, the energy used to calculate HET is not critical to the final MU.

Patient 9 in Table 6 represents an extreme example of the missing lateral scatter which means the TPS must give more MU than the TG-71 calculation. Adding the HET and GF factors brings this calculation under actionable levels. One of our Monte Carlo calculation testbed problems, a 2x2x2 cm^3 block on a flat phantom, can also be represented by the GF corrections presented. Equation 1 with coefficients for 9 MeV from Table 2 gives GF for a 2 cm radius sphere of 0.807. The MU calculated by Eclipse to give 100 cGy to the reference point is 127 MU. The TG-71 MU is 100 MU, a 24 % difference. The corrected MU is 124 MU, a 2 % difference.

While we have used Equation 1 to define the fitting function for GF the fitting function could take on any number of forms. For example, we could have chosen,

Equation 9

$$GF = a\, r^b ,$$

where r is the radius of the sphere and a and b are the fitted coefficients. This form would be simpler to calculate by hand because it has fewer inputs. Also, the mean percent difference for GF from Equation 9, compared to the measured GF in Table 3, is ~1.3%. The mean percent difference for GF using Equation 1 is ~1%. We do not consider this a significant difference. We have settled on Equation 1 because the fit for smaller radius spheres is better, and smaller radius patient geometries will give the larger corrections. We are also able to force the largest radius geometries to return a value less than 1. We will

let the reader decide which form to use. Table 7 presents the fitted coefficients for Equation 9 and are included for completeness.

Table 7: Fitted coefficients for GF based on Equation 9

Energy (MeV)	a	σ_a	b	σ_b
6	0.834	0.011	0.067	0.006
9	0.790	0.010	0.084	0.006
12	0.775	0.010	0.088	0.006

We want to emphasize that not all patient anatomies will be convex. A breast patient with a deficit due to lumpectomy may be concave through one or both planes orthogonal to the beam. In this case, adding a convex curvature correction factor will be inappropriate. Instead, one will need a concave correction factor. We are currently investigating correction factors for concave surfaces. Initial results show the concave factor is roughly the inverse of the convex factor. This makes sense intuitively, but we will forego making further comments in this manuscript.

Conclusion

TG-114 states that MU calculated by hand should be in agreement with MU calculated by the treatment planning system within at most 5 %[4]. This allows for a wide range of materials and patient geometries. HET factors calculated for common materials in Table 5 are 1.00 ± 2 % for all materials except bone. Geometry factors for the calculations presented in Table 6 are 1.00 ± 5 % for the most common cases seen in our clinic. While the action levels in TG-114 are presented as guidelines, it is not unrealistic to

meet those guidelines even for difficult patient geometries and heterogeneities. One must account for all components in the calculation. Algorithms are more advanced, and our second check calculations should be as well. Given the tables presented here the hand calculation still represents a quick, simple, and independent verification of the TPS MU.

1 Gerbi BJ, Antolak JA, Deibel FC, et al. Recommendations for clinical electron beam dosimetry: supplement to the recommendations of Task Group 25. Med. Phys. 2009; **36**(7): 3239–3279.
2 AAPM Radiation Therapy Committee. Task Group, Fraass BA, Doppke K, et al. *Quality Assurance for Clinical Radiotherapy Treatment Planning: Report of the AAPM Radiation Therapy Committee TG#53* (1998).
3 Kisling KD, Ger RB, Netherton TJ, et al. A snapshot of medical physics practice patterns. J. Appl. Clin. Med. Phys. 2018; **19**(6): 306–315.
4 Gibbons JP, Antolak JA, Followill DS, et al. Monitor unit calculations for external photon and electron beams: Report of the AAPM Therapy Physics Committee Task Group No. 71. Med. Phys. 2014; **41**(3): 031501.
5 Stern RL, Heaton R, Fraser MW, et al. Verification of monitor unit calculations for non-IMRT clinical radiotherapy: report of AAPM Task Group 114. Med. Phys. 2011; **38**(1): 504–530.
6 Khan FM. *The Physics of Radiation Therapy* (Lippincott Williams & Wilkins, 2012).
7 Cygler JE, Daskalov GM, Chan GH, Ding GX. Evaluation of the first commercial Monte Carlo dose calculation engine for electron beam treatment planning. Med. Phys. 2003; **31**(1): 142–153.
8 Xu Z, Walsh SE, Telivala TP, Meek AG, Yang G. Evaluation of the eclipse electron Monte Carlo dose calculation for small fields. J. Appl. Clin. Med. Phys. 2009; **10**(3): 2834.
9 Almond PR, Biggs PJ, Coursey BM, et al. AAPM's TG-51 protocol for clinical reference dosimetry of high-energy photon and electron beams. Med. Phys. 1999; **26**(9): 1847–1870.
10 Lichten W. *Data and Error Analysis* (Addison-Wesley, 1999).
11 National Institute of Standards and Technology. *ESTAR, PSTAR, and ASTAR:* (1992).